Photoacoustics 6 (2017) 37–47

Contents lists available at ScienceDirect

Photoacoustics

journal homepage: www.elsevier.com/locate/pacs

Research article

Detection of intramyocardially injected DiR-labeled mesenchymal stem cells by optical and optoacoustic tomography

Markus T. Berninger[a,b,*], Pouyan Mohajerani[c], Moritz Wildgruber[d], Nicolas Beziere[c], Melanie A. Kimm[d], Xiaopeng Ma[c], Bernhard Haller[e], Megan J. Fleming[a], Stephan Vogt[a], Martina Anton[f], Andreas B. Imhoff[a], Vasilis Ntziachristos[c], Reinhard Meier[d], Tobias D. Henning[g]

[a] Department of Orthopaedic Sports Medicine, Klinikum rechts der Isar, Technische Universität München, Munich, Germany
[b] Department of Trauma and Orthopaedic Surgery, BG Unfallklinik Murnau, Murnau, Germany
[c] Institute for Biological and Medical Imaging, Technische Universität München und Helmholtz Zentrum München, Neuherberg, Germany
[d] Department of Radiology, Klinikum rechts der Isar, Technische Universität München, Munich, Germany
[e] Institute for Medical Statistics and Epidemiology, Klinikum rechts der Isar, Technische Universität München, Munich, Germany
[f] Institute for Experimental Oncology and Therapy Research and Institute of Molecular Immunology, Klinikum rechts der Isar, Technische Universität München, Munich, Germany
[g] Section of Neuroradiology, Uniklinik Köln, Cologne, Germany

ARTICLE INFO

Article history:
Received 11 October 2016
Received in revised form 17 April 2017
Accepted 28 April 2017
Available online 4 May 2017

Keywords:
Fluorescence molecular imaging
Multispectral optoacoustic tomography
Rabbit heart
Mesenchymal stem cells
Cell labeling
Intramyocardial injection

ABSTRACT

The distribution of intramyocardially injected rabbit MSCs, labeled with the near-infrared dye 1,1′-dioctadecyl-3,3,3′,3′-tetramethylindotricarbo-cyanine-iodide (DiR) using hybrid Fluorescence Molecular Tomography-X-ray Computed Tomography (FMT-XCT) and Multispectral Optoacoustic Tomography (MSOT) imaging technologies, was investigated.

Viability and induction of apoptosis of DiR labeled MSCs were assessed by XTT- and Caspase-3/-7-testing *in vitro*. 2×10^6, 2×10^5 and 2×10^4 MSCs labeled with 5 and 10 μg DiR/ml were injected into fresh frozen rabbit hearts. FMT-XCT, MSOT and fluorescence cryosection imaging were performed.

Concentrations up to 10 μg DiR/ml did not cause apoptosis *in vitro* ($p > 0.05$). FMT and MSOT imaging of labeled MSCs led to a strong signal. The imaging modalities highlighted a difference in cell distribution and concentration correlated to the number of injected cells. *Ex-vivo* cryosectioning confirmed the molecular fluorescence signal.

FMT and MSOT are sensitive imaging techniques offering high-anatomic resolution in terms of detection and distribution of intramyocardially injected stem cells in a rabbit model.

1. Introduction

Acute myocardial infarction is still the leading cause of morbidity and mortality worldwide, coronary heart disease alone accounts for 46% of all cardiovascular deaths in the US [1]. Although post-infarction survival rates have been improved in recent years, cardiomyocyte loss and subsequently impaired heart function can cause progressive heart failure [2]. The ultimate goal of cardiac repair is to regenerate functional myocardium after injury to prevent or treat heart failure. Unfortunately, the capacity of self-regeneration of myocardial tissue is limited in primates [3]. This limited capacity has led to the introduction of gene- and cell-based therapeutic approaches, which aim at replenishing the diminished myocytes to achieve a new myocardium that is electrically and mechanically integrated into the contractile unit and their assembly [4].

Cell-based cardiac regenerative therapy offers a promising therapy for myocardial infarction. However, the optimal cell type to achieve this goal has not been established yet [5–13]. In particular, bone marrow derived mesenchymal stem cells (MSCs) have been extensively investigated as a potential therapeutic approach for cardiac regeneration due to their distinctive characteristics [14–16]. Originally, it was asumed that MSCs engrafted in the myocardium differentiate into cardiomyocytes and could, therefore, lead to direct cellular cardiac regeneration

* Corresponding author at: Department of Trauma and Orthopaedic Surgery, BG Unfallklinik Murnau, Prof.-Küntscher-Strasse 8, 82418, Murnau, Germany.
E-mail address: Markus.Berninger@bgu-murnau.de (M.T. Berninger).

http://dx.doi.org/10.1016/j.pacs.2017.04.002

[17]. Current evidence, however, has led to the assumption that MSCs act in a paracrine manner through the release of cytokines [18,19].

In recent years, cardiac repair has moved rapidly from studies in experimental animals to clinical trials involving thousands of patients [20,21]. Clinical trials using bone marrow cells have demonstrated the safety and feasibility of myocardial transplantation of stem cells, but have yielded moderate if any results in terms of a therapeutic benefit [22–30].

The clinical promise for stem cell therapy in ischemic heart disease will not be fully attained without an improved understanding of stem cell biology and mechanisms of repair and regeneration. A noninvasive assessment of the survival, distribution and differentiation of the MSCs will be necessary to monitor the transplanted cells in the same subject over time. The development of imaging tools that allow longitudinal assessment of the fate of injected stem cells with high spatial resolution and the ability to simultaneously determine cellular viability, represents one of the current goals for these therapeutic approaches. Magnetic resonance imaging (MRI) [31,32], positron emission tomography (PET) [33,34] and single-photon emission computed tomography (SPECT) [35,36] with clinically approved contrast agents and reporter genes have already been tested in various clinical trials of cell tracking in myocardial regeneration. However, none of these clinically established imaging modalities fulfilled the above mentioned criteria.

In the last years, optical imaging in the near-infrared (NIR) spectrum has played an increasing role in cardiovascular research [37–39]. Noninvasive optical imaging of macrophage infiltration using fluorescent nanoparticles [40] and investigations of monocyte recruitment for infarct healing [41,42] have been performed using fluorescence molecular tomography (FMT). However, the accuracy of stand-alone FMT, which has demonstrated highly sensitive imaging of molecular probes, suffers due to the strong scattering of emitted photons and/or light in turbid media of biological tissue [43,44]. FMT in combination with CT – a hybrid modality called FMT-XCT – further improves high morphological, three-dimensional detail [45,46].

Alternatively, optoacoustic imaging, and in particular, multispectral optoacoustic tomography (MSOT) has been proposed to noninvasively achieve high-resolution maps of various fluorescent contrast agents several centimeters deep in tissue [47,48]. It is capable of greatly improving the resolution over pure optical methods because typically it is not hindered by optical scattering. MSOT images purely rely on the conversion of light energy into ultrasound through the photoacoustic effect provided by chromophores [47]. In preclinical studies, this technology has already successfully been used to image heart and blood vessels in a mouse model [49,50]. Both MSOT and FMT present characteristics that other modalities classically used for cardiac cell tracking do not: in particular they are both highly sensitive imaging modalities devoid of ionizing radiations, and both allow for longitudinal assessment due to the inherent stability of the dye chosen [51,52]. These imaging modalities are promising to rapidly translate major findings in cell and molecular biology to more complex models and to further investigate biological processes during myocardial healing *in vivo* and to evaluate novel therapeutic strategies.

The aim of this work was a proof of concept study to establish highly sensitive and easy to use preclinical imaging techniques of FMT and MSOT without the use of ionizing radiation. Therefore, this study investigated the distribution of intramyocardially implanted rabbit MSCs, labeled with the near-infrared dye 1,1′-dioctadecyl-3,3,3′,3′-tetramethylindotricarbo-cyanine iodide (DiR), at different concentrations and cell numbers using both FMT-XCT and MSOT technologies. The implementation of these imaging modalities for cardiac cell tracking might advance the field of cell-based cardiac regenerative therapy and form the basis for further studies including potential prospective clinical applications, *e.g.* examination of inflammation in atherosclerotic plaques in relatively superficial arteries, or via an intravascular imaging approach [49].

2. Material and methods

All animal experiments were reviewed and approved by the Animal Research Authority of the government of Upper Bavaria (AZ 105-11) and were performed in accordance with the U.S. National Institutes of Health guidelines for the care and use of laboratory animals [53].

2.1. Cell-labeling with DiR

For cell labeling, bone marrow-derived mesenchymal stem cells (MSCs) were collected from a 4 month-old male New Zealand White rabbit, as described previously [54]. All MSCs were used at passage 2–4 in order to prevent senescence. MSCs were labeled using Xenolight DiR (Perkin Elmer, Rodgau, Germany), a NIR lipophilic carbocyanine dye excited at 750 nm, with an emission peak at 782 nm [55]. Parallel triplicate samples of 1×10^6 cells/ml were incubated with different concentrations of DiR (1.25, 2.5, 5.0 and 10 μg DiR/ml) in a volume of 1 ml 1xPBS for 30 min at 37 °C. 3 ml serum-free culture medium were added to each sample and cells were washed twice with PBS by centrifugation (1200 rpm, 3 min, 25 °C) to remove non-incorporated dye. Similarly treated unlabeled cells served as controls.

Fluorescence intensity of MSC labeled with 10 μg DiR/1×10^6 MSC was analyzed by flow cytometry (Cyan ADP, Beckman Coulter, Krefeld, Germany) on channel APC-Cy7 within the whole cell population (single-parameter histogram) using FlowJo software (Tree Star, Ashland, OR, USA). To analyze the localization of the dye within the MSC, fluorescence microscopy of labeled cells was performed. Cells were labeled with 5 and 10 μg DiR/ml, respectively, and cultured for 24 h on slides. Then, cells were fixed with 4% PFA (Carl Roth GmbH, Karlsruhe, Germany) and labeled with DAPI (4′,6-Diamidin-2-phenylindol; Life Technologies, Darmstadt, Germany). Finally, fixed cells were analyzed using a fluorescence microscope (Axio Imager Z1, Zeiss GmbH, Jena, Germany).

2.2. Cell viability and toxicity screening

Cellular proliferation rate and viability of labeled cells were tested using the Cell Proliferation Kit II (XTT) (Roche Diagnostics, Mannheim, Germany) [56]. After cell labeling and the described washing steps, the cells were incubated with the XTT reagent mixture for 18 h in a humidified atmosphere. Afterwards, cell viability was spectrophotometrically quantified by measuring the absorbance using a multi-label plate reader (PerkinElmer Inc., Rodgau, Germany).

For assaying apoptosis (caspase-3/-7 activities), the SensoLyte® Homogeneous AMC Caspase-3/7 Assay Kit (Anaspec, MoBiTec, Göttingen, Germany) was used [57]. After incubation for 18 h, fluorescence was measured at excitation/emission wavelengths of 355/430 nm. Camptothecin treated cells (5 μM) were used as positive controls.

2.3. Intramyocardial injection of DiR labeled MSCs

Two fresh frozen rabbit hearts were prepared for injection of MSCs labeled with 5 and 10 μg DiR/ml, respectively (Fig. 1). The hearts were perfused thoroughly with PBS to remove adherent blood. The left ventricle was localized and divided into four

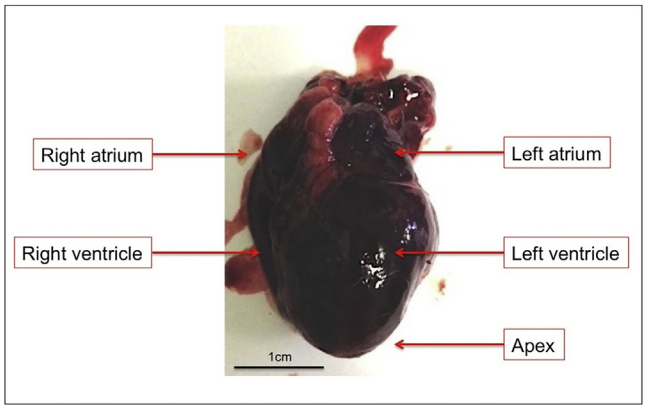

Fig. 1. Heart of a New Zealand White rabbit, right after explantation with left ventricle seen at the front. Subsequently, the heart was washed thoroughly with PBS to remove all soluble blood.

quadrants, which were initially marked by sutures. DiR-labeled cells were centrifuged at 1200 rpm for 3 min, re-suspended in 50 μl PBS and slowly injected into four different quadrants. 2×10^6, 2×10^5 and 2×10^4 DiR-labeled MSCs were implanted, respectively. 2×10^6 unlabeled cells served as control. FMT-XCT and MSOT imaging were performed directly afterwards.

2.4. FMT-XCT

A fluorescence molecular tomography-X-ray computed tomography (FMT-XCT) hybrid imaging system was used to image the samples. The FMT-XCT system has been described in details in [58]. Briefly, the system operates in 360° *trans*-illumination geometry, where the sample was illuminated by a 750 nm laser at 18 equally spaced gantry locations, where images were acquired at both excitation and fluorescence wavelengths of DiR (~750 and ~830 nm, respectively) using a CCD cooled at −80 °C. The optical part of the FMT-XCT imaging lasted around 50 min per sample. CT imaging was performed afterwards using the X-ray sub-system of the FMT-XCT, consisting of an eXplore Locus micro-CT scanner (GE Healthcare, U.K.) covering a scan field of ~40 mm in the axial direction. The CT acquisition lasted ~20 min per sample. The FMT-XCT system was modeled using a finite-element approach, accounting for light propagation. Anatomical information was used in conjunction with optical data for improved accuracy using a regularized linear least squares approach [46,58].

2.5. Fluorescence cryosection imaging

For validation of the *ex vivo* imaging results, fluorescence cryosection imaging was performed of the excised heart after embedding in Tissue-Tek® O.C.T. (TM) (Sakura Finitek Europe B. V., Zoeterwonde, Netherlands) to map the fluorescence signal originating from DiR. The frozen heart was sliced in the short axis at a 500 μm micron pitch. Color and fluorescence images were recorded for each slice. The cryosection imaging system is based on a cryotome (CM 1950, Leica Microsystems, Wetzlar, Germany), fitted with a motorized spectral illumination and multi-spectral CCD-based detection in *epi*-illumination mode [59]. Fluorescence images were captured at the peak emission wavelength of DIR at 782 nm.

2.6. Multispectral optoacoustic tomography (MSOT)

All MSOT measurements were performed using a MSOT inVision 256-TF system (iThera Medical, Munich, Germany). Optical excitation was provided by a laser, with a pulse-duration of around 10 ns and a repetition rate of 10 Hz, within a tunable range of 680–980 nm and an average energy of 80 mJ per pulse. A fiber bundle split into 10 output arms was used to achieve the homogeneous delivery of light to the sample in a ring formation. The detection and record of emitted ultrasound waves was obtained by means of a 256 element transducer array cylindrically focused and having a central frequency of 5 MHz, allowing acquisition of transverse plane images. A moving stage enabled the imaging of different planes by the static illumination and detection devices. Measurements were executed in a temperature controlled water bath (34 °C) for acoustic coupling and to keep the sample dry, a clear polyethylene membrane attached to the sample holder was employed [60]. Processing of the data acquired during the imaging experiments was performed using the viewMSOT software (iThera Medical, Munich, Germany). Volume estimation of the cell distribution was performed by selecting pixels with a DiR optoacoustic signal value above background and approximating the shape to an ellipsoid, using the surface of the signal distribution in the most intense image times the distance between the two images containing signal from the same injection location. Maximum value in combination with volume was used to give insight into how far the cells went (volume) and how many remained at the injection spot (maximum).

2.7. Statistical analysis

Statistical calculations were performed using the statistical software R 3.1.1 (Release date 2014, Vienna, Austria) and GraphPad Prism 5.04 (Release date 2010, San Diego, CA, USA). Measurements of cell viability and toxicity were acquired in triplicates. Mean values and standard deviations were calculated. Labeled samples were compared with untreated controls using a linear regression model treating concentration as factor. A two-sided 5%-level of significance was used for all tests. MSOT error bars are derived from different data spectral unmixing methods (principal component analysis, linear regression methods using different reference spectra).

3. Results

3.1. Cell labeling and in vitro analysis of viability and apoptosis

Fig. 2 shows uniform labeling of MSCs with 10 μg/ml DiR as analyzed by flow cytometry (Fig. 2A) and fluorescence microscopy (Fig. 2B and C). Concentrations up to 10 μg/ml DiR/ml did not change cell viability or cause apoptosis *in vitro* (Fig. 3). In comparison to unlabeled controls (1.63 ± 0.16), cells labeled with DiR concentrations of 1.25 and 2.5 μg DiR/ml showed a non-significant increase in cell metabolism (1.79 ± 0.17, $p = 0.264$ and 1.82 ± 0.17, $p = 0.184$). In contrast, 5.0 and 10 μg DiR/ml led to a decrease in metabolism (1.45 ± 0.17, $p = 0.201$; 1.27 ± 0.15, $p = 0.022$) (Fig. 3A). Fig. 3B reveals that none of the concentrations led to an increase in caspase-3/-7-activity ($p > 0.05$, each). However, all samples were significantly different to the apoptotic positive control Camptothecin ($p < 0.001$, each).

3.2. Fluorescence molecular tomography (FMT)

FMT of labeled, intramyocardially injected MSCs showed a strong signal at the four injection points (Figs. 4 and 5). Each signal intensity (in a.u.) was matched to the one measured at the injection site of MSCs labeled with 2×10^6. While FMT imaging of the rabbit heart with injected cells labeled with 5 μg DiR/ml (Fig. 4) revealed a dose-dependent signal within the varying cell numbers, imaging of the rabbit heart with injected cells labeled with 10 μg DiR/ml

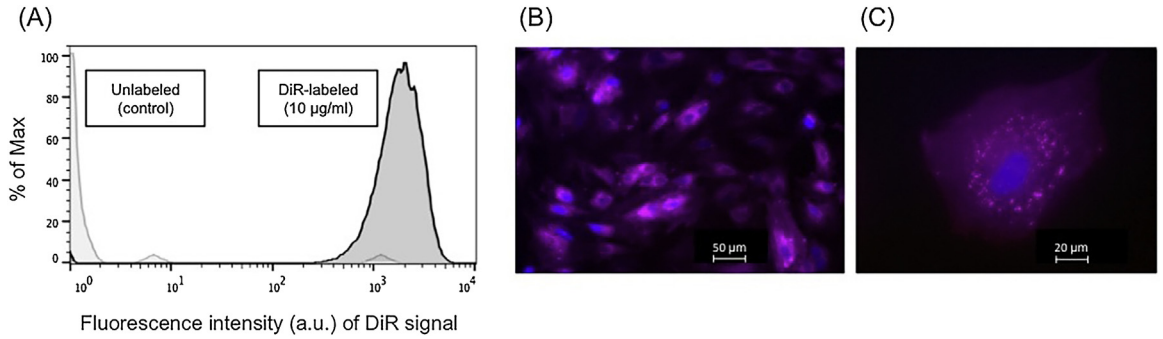

Fig. 2. (A) Flow cytometric analysis of labeling efficiency of rabbit MSCs, exemplarily for dye concentration of 10 µg/ml DiR. Light grey = unlabeled control cells, black = DiR labeled MSCs. Histogram overlay shows fluorescence intensity of the DiR signal measured on the APC-Cy7 channel (log scale) on the X-axis. The fluorescence intensity is an arbitrary unit (a.u.). The Y-axis shows the number of cells normalized to mode (percent of max; scaling each curve to 100%). (B, C) Fluorescence microscopy of rabbit MSC labeled with 10 µg DiR/ml (B: 10× magnification; C: 40× magnification). Nuclear counterstaining was performed with DAPI (blue staining).

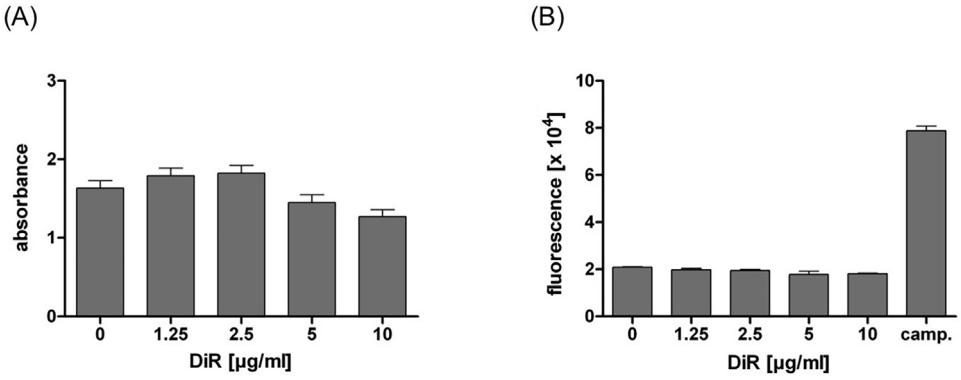

Fig. 3. (A) XTT-test and (B) caspase-3/-7 test of different DiR concentrations. Concentrations up to 10 µg/ml DiR/ml did not significantly change cell viability or cause apoptosis *in vitro*. All samples were significantly different to the apoptotic positive control Camptothecin ($p < 0.001$, each). Absorbance was expressed as A_{490nm}–A_{630nm} and fluorescence as relative fluorescence units ($\times 10^4$), respectively.

(Fig. 5) indicated a stronger signal intensity at the location of injection of 2×10^4 cells compared to the location of 2×10^5 cells. The injection of 2×10^6 resulted in the strongest signal while reduced cell numbers led to minor signal intensity. Unlabeled cells had a signal intensity of 0.11 a.u. (Fig. 4) and 0 a.u. (Fig. 5).

Interestingly, an injection of MSCs labeled with a higher fluorescent dye concentration (10 µg DiR/ml) resulted in an attenuated signal compared to 5 µg DiR/ml.

3.3. Fluorescence cryosection imaging

The results of the fluorescence cyrosection imaging were in line with FMT findings; especially concerning signal intensity and dose-dependence within the varying cell numbers. As seen in Fig. 4 and 5, both FMT-XCT and cryosection images reveal signals in similar and comparable anatomical locations.

3.4. Multispectral optoacoustic tomography (MSOT)

Multispectral optoacoustic images of the DiR-MSCs injected rabbit hearts are presented in Fig. 6 and 7. DiR signal, identified after signal unmixing, can be detected at 3 different locations in a diffuse pattern (highlighted in the figure), with an additional bright spot at what appears to be the injection site at a different depth in the muscle tissue. A fly-through video (see Supplementary material) illustrating the top to the apex in half-millimeter steps, allows for accurate rendering of these patterns. Quantification of the optoacoustic signal obtained from the injection sites is shown in the bar graphs for the two different samples. The maximum signal intensity appears to correlate with the number of labeled cells injected, as it represents the signal intensity in the few pixels at precisely the injection location. In both samples labeled with different DiR concentrations, the background DiR signal was around 10 a.u., while the labeled cells provided from 20 to 40 a.u. of maximum DiR signal depending on the number of cells injected. The maximum values obtained in both samples with different DiR labeling methods did not provide any significant difference.

The volume holding signal is superior to the background DiR signal, approximated assuming an ellipsoid distribution does not appear to increase with the number of cells injected but rather decrease. As with the maximum DiR optoacoustic, the values obtained did not differ between labeling methods and stayed between 100 and 200 mm^3 (compare Figs. 6 and 7).

4. Discussion

In our study, we could successfully image the distribution of intramyocardially injected rabbit MSCs labeled with the near-infrared dye 1,1′-dioctadecyl-3,3,3′,3′-tetramethylindotricarbo-cyanine iodide (DiR), using both FMT-XCT and MSOT technologies.

FMT of the myocardium was first performed in mice after uptake of magnetofluorescent nanoparticles (CLIO-Cy5.5) by

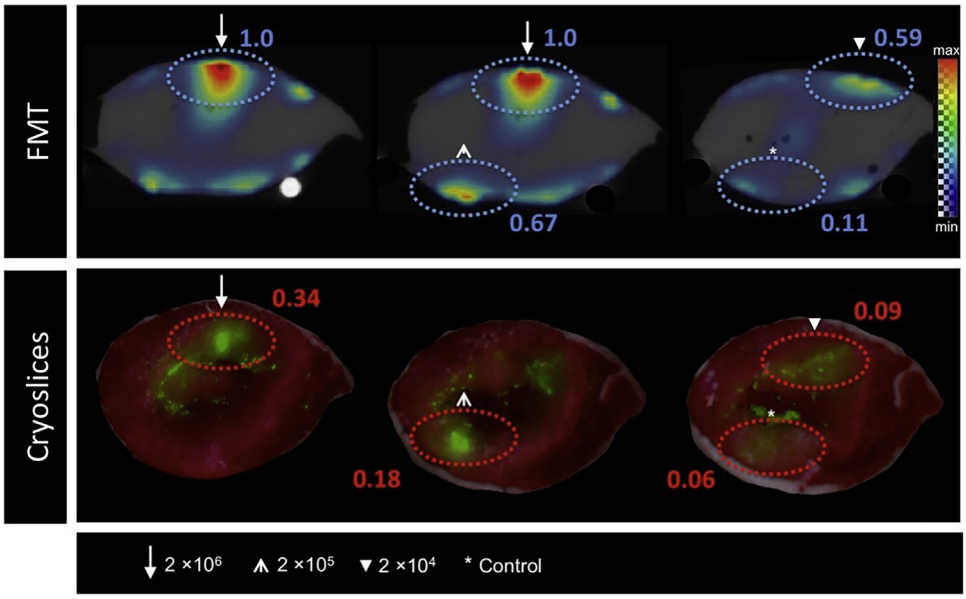

Fig. 4. FMT (top) and fluorescence cryosection images (bottom) of a rabbit heart after left-ventricular injection of 2×10^4, 2×10^5 and 2×10^6 MSCs labeled with 5 μg DiR/ml. Injection of unlabeled cells served as control. The four spotted, oval circles in each slide highlight the injection areas of the cells. On the FMT images, the largest signal (max) is mapped to the red color with zero transparency and the lowest signal (min) is mapped to the blue color with full transparency. On the cryosection images the largest signal is mapped to the green color with no transparency and the lowest signal to the green color with full transparency.

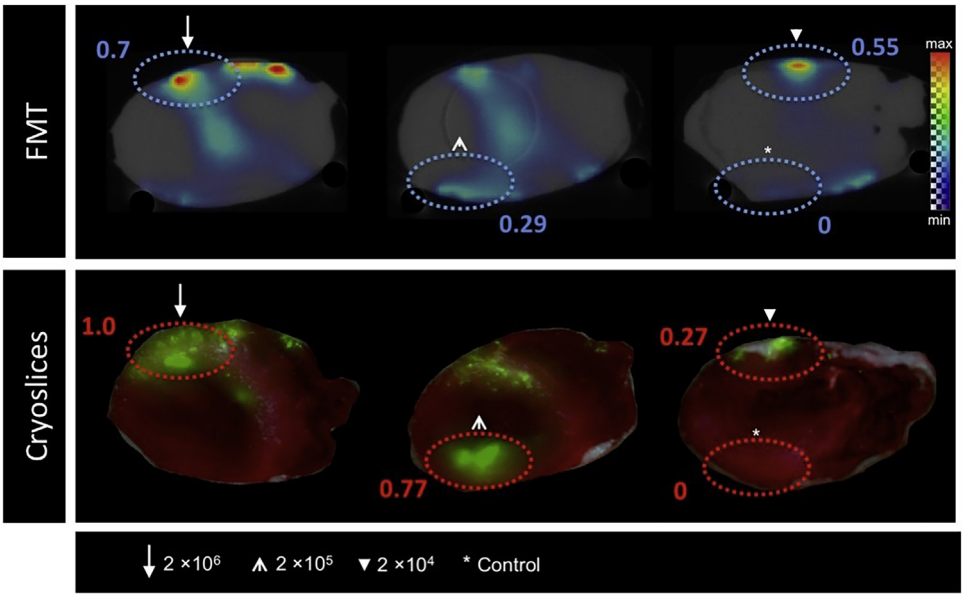

Fig. 5. FMT (top) and fluorescence cryosection images (bottom) of a rabbit heart after left-ventricular injection of 2×10^4, 2×10^5 and 2×10^6 MSCs labeled with 10 μg DiR/ml. Injection of unlabeled cells served as control. The four spotted, oval circles in each slide highlight the injection areas of the cells. For explanation of the color bar see Fig. 4.

macrophages in infarcted myocardium [40]. In this study the FMT signal increased linearly with the dose of CLIO-Cy5.5 injected similarly to the signal seen in T2*-weighted MRI. Furthermore, extensive monocyte recruitment around infarcted areas [41,42] and impaired recruitment of phagocytes and protease activity have been observed using FMT [61]. Ale et al. showed that FMT-XCT is able to detect apoptosis noninvasively and *in-vivo* in the healing myocardium by quantification of Annexin-Vivo750, a florescent imaging agent [62]. These studies showed the potential of FMT to be of significant value in research and thereby, in clinical settings one day, too, and may play an important role in the study of post-infarction healing. Beside the high spatial resolution and potential longitudinal assessment achieved by FMT, we assume that our intermediate sized rabbit model offers pronounced imaging quality through higher image detail compared to smaller animals. However, even in the near-infrared portion of the spectrum, significant absorption and scattering of light limit penetration to a few centimeters. This limits fluorescence imaging in humans to superficial structures or invasive techniques. Thus, fluorescence imaging of the human heart will likely require surgical or catheter-based approaches in the foreseeable future [63].

Optoacoustic imaging has been proposed as an alternative for imaging the optical characteristics of tissue [64–66]. As opto-acoustic imaging only suffers marginally from optical scattering, it is capable of greatly improving the resolution over pure optical methods and combines the high contrast obtained from optical

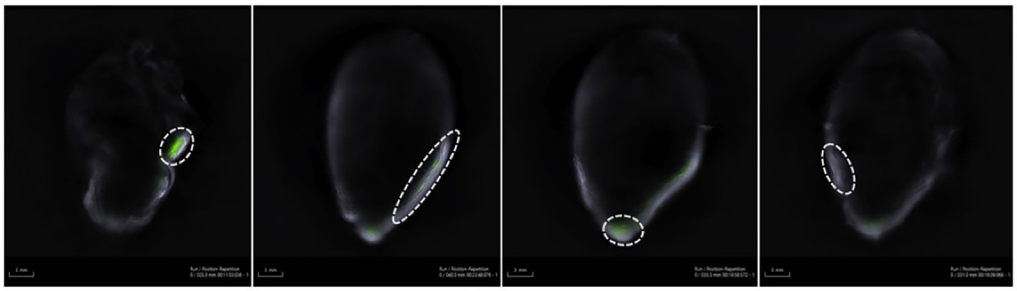

Z position (mm)	25	40	35.5	31
Injected cell number	2 x 10^6	2 x 10^5	2 x 10^4	2 x 10^6 (control)

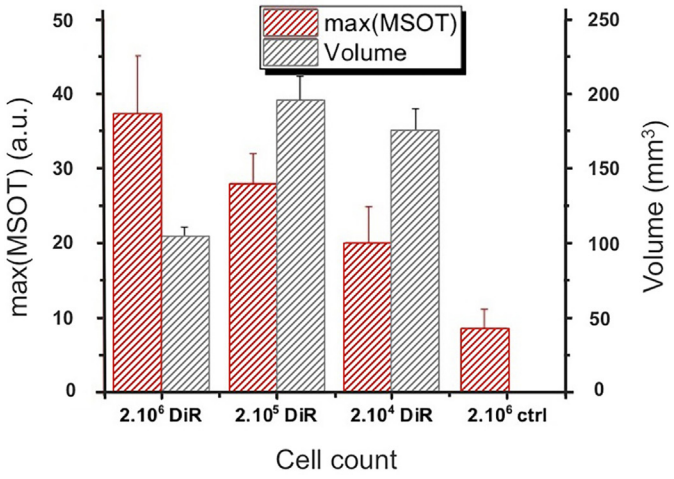

Fig. 6. Optoacoustic imaging of three injection sites located in the heart (25; 35,5 and 40 mm) and a reference injection site (31 mm). MSCs were labeled with 5 μg DiR/ml. Top row: Multispectral optoacoustic images of the DiR signal (green) overlayed on the 800 nm image (grey scale). Bar graph: Maximum MSOT signal (a.u.) detected at the injection sites (red); volume in which the DiR signal was superior to background signal (black).

absorption with the high resolution of ultrasonic detection. Molecular imaging has been further enabled using optoacoustic techniques via spectral unmixing methods. In particular, MSOT has been proposed to noninvasively achieve high-resolution maps of molecular agents, such as fluorochromes [67] and fluorescent proteins [68], and other chromophores [47,69] several centimeters deep in tissue [47,48], well suited for cardiac imaging.

The intrinsic contrast of stem cells relative to native heart tissue is very low. Thus, prior to transplantation the MSCs were directly labeled with the fluorophore DiR to enable their detection relative to the surrounding tissue either based on its fluorescence for FMT and planar fluorescence, or on its absorbance for MSOT. Literature shows that as few as 10.000 monocytes labeled with DiR could be detected by fluorescent imaging [70] while the lowest detectable cell number in this study was much lower than normally applied cell numbers in clinical trials [71,72]. Currently, direct labeling techniques *in vitro* prior to transplantation serve as the primary means of labeling stem cells for *in vivo* cardiovascular applications compared to receptor-based or reporter gene labeling techniques [73]. DiR has previously been described to show a high emission wavelength compared to other lipophilic membrane dyes [74]. DiR presents a detection sensitivity being strong enough even for the deep part of an organ, *e.g.* the myocardium or even endocardium, and therefore, it is very suitable for such an intramyocardial experimental model. In our study, concentrations up to 10 μg/ml DiR/ml did not significantly change cell viability or cause apoptosis *in vitro*. In literature, recently published studies revealed the suitability of DiR for *in vivo* long-term cell tracking. Youniss et al. demonstrated persistence of fluorescent signal associated with DiR labeled T-cells for 3 weeks post labeling *in vivo* in a mouse model using multi-spectral fluorescent imaging [51]. Du et al. observed concentrated fluorescence signals for a minimum of two weeks at the tumor site infused with DiR labeled human cytokine-induced killer cells and cytotoxic T lymphocytes in a mouse model of gastric carcinoma [52].

In our study, we presented the application of MSOT techniques to image labeled MSCs implanted in a rabbit heart. The anatomical resolutions, which were achieved by this imaging modality, are not possible with current deep-tissue optical imaging methods. However, the resolution of anatomical structures (*e.g.* coronary vessels, septum *etc.*) plays an important role in the research and diagnosis of cardiovascular diseases. The ability of optoacoustic imaging to highly resolve these anatomical structures allows for promising cardiac applications, in real-time and *in vivo*. Preclinically, this technology has successfully demonstrated anatomical visualization of heart and blood vessels of mice [49,50].

The results of our proof of principle study showed that FMT of labeled, intramyocardially injected MSCs led to a strong signal at

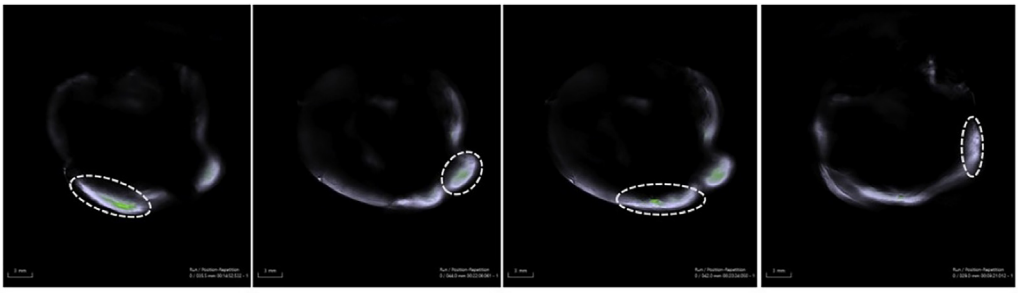

Z position (mm)	35.5	44	52	29
Injected cell number	2 x 10^6	2 x 10^5	2 x 10^4	2 x 10^6 (control)

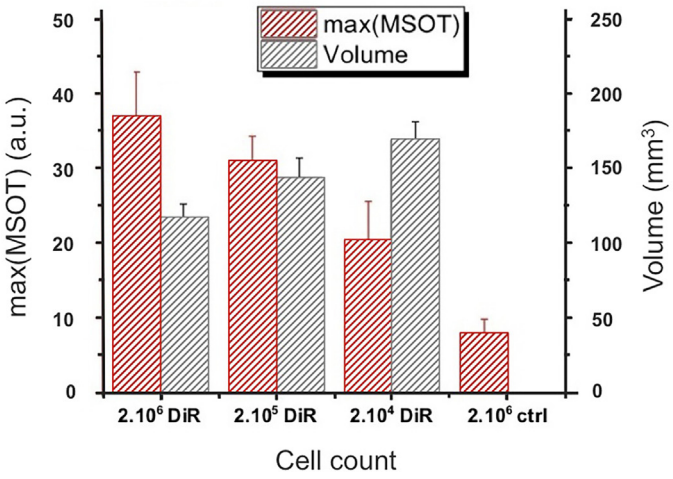

Fig. 7. Optoacoustic imaging of three injection sites located in the heart (35,5; 44 and 52 mm) and a reference injection site (29 mm). MSCs labeled with 10 μg DiR/ml. Top row: Multispectral optoacoustic images of the DiR signal (green) overlayed on the 800 nm image (grey scale). Injection locations circled for clarity. As the two injection sites presented in the second and third panel were close (approximately 5 mm Z distance in the position the heart was in), the DiR signal present outside of the circled area in the third panel comes from remaining cells of the injection site shown in the second panel. Bar graph: Maximum MSOT signal (a.u.) detected at the injection sites (red); volume in which the DiR signal was superior to background signal (black).

the four injection points and thereby, allows for visualization of DiR-labeled MSCs after their injection in rabbit hearts. Additional *ex-vivo* cryosectioning confirmed the molecular fluorescence signal in the myocardium. Signal localization in the *ex-vivo* cryoslices did not always match exactly the FMT-XCT images, as it is not possible to keep the rabbit heart geometry identical between imaging and the freezing of the heart [50]. Both FMT-XCT and cryosection images revealed signals in similar and comparable anatomical location. The attenuated signal in FMT-XCT imaging at a higher fluorescent dye concentration was most likely due to quenching. The effect of fluorescent quenching of DiR has previously been described by Cho et al. [75]. The authors showed that fluorescence intensities of DiR in PEG-*b*-PCL micelles were concentration-dependent. Depending on the extent of DiR incorporation, DiR existed in either a quenched or non-quenched state in the cores of the micelles resulting in different fluorescent intensities. Therefore, quenching is conceivable for this effect here, too. Fluorescence quenching should have close to no impact of optoacoustic signal strength because only the absorbed photons will generate optoacoustic signal. In the case of DiR, as with all red shifted cyanine derivatives, the fluorescent yield is already low (<5%), leaving most of the absorbed light energy available for optoacoustic signal generation. In the case of re-emitted and re-re-absorbed light (quenching), we can assume those photons will generate extra optoacoustic signal. Furthermore, a discrepancy of signal intensity between the varying cell numbers was observed in FMT imaging of the heart after injection of MSCs labeled with 10 μg DiR/ml. This discrepancy might be due to unaccounted signal of local optical heterogeneity around this particular location of 2×10^5 cells inside the sample. Specifically, our implementation of FMT-XCT for this work assumes homogeneous optical absorption and scattering in the entire volume of the tissue sample. Any strong optical heterogeneity, such as due to remaining high blood/hemoglobin concentration in a particular location, can perturb the validity of the FMT model and result in artifacts or erroneous reconstructions.

Using MSOT, we could identify DiR signal intensity variation between the injection locations that could be divided in two metrics: maximum signal intensity, extracted from the voxel bundle pertaining to the injection point, and volume containing positive DiR signal. Maximum MSOT signal provided a clear correlation with the number of cells injected as well as with the values extracted from strictly fluorescent imaging techniques, with signal intensities growing with the number of cells injected. DiR signals from the injected cells could clearly be identified above background signal, which was equal to the signal obtained from

the injection location of the reference cells. The non-negligible standard deviation stems from the difficult setting: with a relatively thick muscle, non-homogeneous distribution of the cells and presence of remaining hemoglobin, variation in light fluence becomes predominant in signal accuracy and is heavily dependent on orientation and positioning of the sample in the imaging cavity.

In an attempt to circumvent the resulting quantification issues, we evaluated the volume occupied by the DiR labeled cells in the heart tissue by estimating the volume of an ellipsoid containing DiR signal around each injection site. Interestingly, the diffusion of the cells in the muscle tissue appears to be favored when a more diluted suspension is injected. Overall, the MSOT results correlated nicely with the FMT and cryosection fluorescence imaging results coincidentally also providing real time imaging not possible with fluorescence methods.

In the context of *in vivo* cell tracking studies it is important to recognize the problem of dye transfer. Implanted labeled cells may die, release the contrast agent, which might then be taken up by macrophages and thus cause persisting imaging signal in the target organ. This imaging signal mimics successful cell engrafting but actually represents cell death. The problem is well recognized, also with other imaging techniques as magnetic cell labeling for MR imaging [76–79]. Some studies have thus focused on generating a functional imaging signal to detect death of the implanted cells be compartmentalization effects [80]. Ricles et al. have developed a technique to discriminate macrophages from implanted mesenchymal stem cells *in vivo* by a dual gold nanoparticle system for cell tracking based on labeling with different nanoparticles and photoacoustic imaging [81]. However, the ultimate goal would be to reduce the rate of cell death by improving cell transplantation techniques. This includes, for instance, tissue-engineering strategies with scaffolds of natural or synthetic polymers [82] or fibrin gels [83] as well as preconditioning and genetic modification of MSCs which can enhance the resistance of MSCs against hypoxia, oxidation, and inflammation [84,85]. In fact, while some studies describe up to a 99% rate of cell death after transplantation after a few days [17] newer studies report rates below 85% within 7 days [86]. Another solution might be systemic application of labeled cells [87,88] as unspecific uptake of released contrast would then be systemic and imaging signal in the target organ would thus predominantly represent successful cell engrafting.

Several limitations pertain to our study. Being a proof of principle study, the sample number ($n = 2$) was limited. However, the ultimate goal of this study was to evaluate if visualization of implanted cells by FMT-XCT and particularly by MSOT in a heart of an intermediate animal model is possible at all. Our results demonstrated that this goal is achievable. This study lacks an additional analysis of a tissue-mimicking phantom to clarify quantitative analysis of optoacoustic signal generation from the labeled cells with minimized effects of other factors such as background signals and errors in volume measurement and cell number estimation. However, our previous and preliminary experiments with dye in phantoms showed that we could detect and estimate rather easily and linearly the concentration and shape distribution of built-in dye. Ultimately though, the transition to our animal model, its peculiar shape and non-homogeneity could not be reproduced as accurately as in a phantom. Therefore, future studies should address these aspects more profoundly. Moreover, imaging was performed with freshly explanted hearts and not in a living animal. Therefore, follow-up analyses of the implanted cells were not possible and our study serves, for this part too, as proof of principle only. Future work will have to visualize fluorescent cells at later time points.

5. Conclusions

In summary, our work shows that both FMT-XCT and MSOT are practical applications in preclinical research of cell-based cardiac regenerative therapy in terms of detection and distribution of injected stem cells in hearts of an intermediate sized rabbit animal model with additional high-resolution anatomical information. These imaging modalities, however, can be used to rapidly translate major findings in cell and molecular biology to more complex *in vivo* models. Intermediate animal studies could apply MSOT together with targeted fluorescent agents, *e.g.* DiR, to further investigate biological processes during myocardial healing *in vivo* and to evaluate novel therapeutic strategies. MSOT imaging could eventually find diverse use in clinical settings, owing in particular to its video-rate imaging capacity. Potential applications include the examination of inflammation in atherosclerotic plaques in relatively superficial arteries, or via an intravascular imaging approach [49]. We believe that at the current state of the technologies used, MSOT has an advantage in terms of acquisition convenience and volumetric accuracy, while FMT remains more sensitive. Therefore, we believe complete preclinical studies would thus be better served by combining the two imaging modalities. Molecular imaging modalities like FMT or MSOT may help to first understand, and then control and monitor the healing process of myocardial infarction evoked by injection of mesenchymal stem cell into myocardial tissue.

Conflict of interest

None.

Acknowledgements

This work was supported in part by the German Research Foundation (DFG, HE 4578/3-1, ME 3718/5-1 and ME 3718/2-1) and in part by the BMBF (Federal Ministry of Education and Research, Germany) excellence cluster m^4 (BMBF M4 PM8 801EX1021D). This work was supported by the DFG Cluster of Excellence “Nanosystems Initiative Munich (NIM)”, by the European Union 7th Framework Programs BrainPath (PIAPP-GA-2013-612360) and FMT-XCT (FP7 HEALTH, Contract 201792) and by the European Research Council under the European Union's Seventh Framework Programme (FP/2007-2013)/ERC Grant Agreement no. [233161].

References

[1] D. Mozaffarian, E.J. Benjamin, A.S. Go, et al., Heart disease and stroke statistics-2016 update: a report from the american heart association, Circulation 133 (4) (2016) e38–e360.
[2] J.B. Young, M.E. Dunlap, M.A. Pfeffer, et al., Mortality and morbidity reduction with Candesartan in patients with chronic heart failure and left ventricular systolic dysfunction: results of the CHARM low-left ventricular ejection fraction trials, Circulation 110 (17) (2004) 2618–2626.
[3] G.C. Fonarow, Heart failure: recent advances in prevention and treatment, Rev. Cardiovasc. Med. 1 (1) (2000) 25–33 54.
[4] N.M. Caplice, A. Deb, Myocardial-cell replacement: the science, the clinic and the future, Nat. Clin. Pract. Cardiovasc. Med. 1 (2) (2004) 90–95.
[5] J. Muller-Ehmsen, P. Whittaker, R.A. Kloner, et al., Survival and development of neonatal rat cardiomyocytes transplanted into adult myocardium, J. Mol. Cell. Cardiol. 34 (2) (2002) 107–116.
[6] T.I. Fuentes, N. Appleby, E. Tsay, et al., Human neonatal cardiovascular progenitors: unlocking the secret to regenerative ability, PLoS One 8 (10) (2013) e77464.
[7] D.A. Taylor, B.Z. Atkins, P. Hungspreugs, et al., Regenerating functional myocardium: improved performance after skeletal myoblast transplantation, Nat. Med. 4 (8) (1998) 929–933.
[8] T. Siminiak, R. Kalawski, D. Fiszer, et al., Autologous skeletal myoblast transplantation for the treatment of postinfarction myocardial injury: phase I clinical study with 12 months of follow-up, Am. Heart J. 148 (3) (2004) 531–537.

[9] N. Hassan, J. Tchao, K. Tobita, Concise review: skeletal muscle stem cells and cardiac lineage: potential for heart repair, Stem Cells Transl. Med. 3 (2) (2014) 183–193.

[10] J.Y. Min, Y. Yang, M.F. Sullivan, et al., Long-term improvement of cardiac function in rats after infarction by transplantation of embryonic stem cells, J. Thorac. Cardiovasc. Surg. 125 (2) (2003) 361–369.

[11] J.J. Chong, X. Yang, C.W. Don, et al., Human embryonic-stem-cell-derived cardiomyocytes regenerate non-human primate hearts, Nature 510 (7504) (2014) 273–277.

[12] D. Orlic, J. Kajstura, S. Chimenti, et al., Bone marrow cells regenerate infarcted myocardium, Nature 410 (6829) (2001) 701–705.

[13] C.E. Murry, M.H. Soonpaa, H. Reinecke, et al., Haematopoietic stem cells do not transdifferentiate into cardiac myocytes in myocardial infarcts, Nature 428 (6983) (2004) 664–668.

[14] A.A. Mangi, N. Noiseux, D. Kong, et al., Mesenchymal stem cells modified with Akt prevent remodeling and restore performance of infarcted hearts, Nat. Med. 9 (9) (2003) 1195–1201.

[15] L.C. Amado, A.P. Saliaris, K.H. Schuleri, et al., Cardiac repair with intramyocardial injection of allogeneic mesenchymal stem cells after myocardial infarction, Proc. Natl. Acad. Sci. U. S. A. 102 (32) (2005) 11474–11479.

[16] R. Rahbarghazi, S.M. Nassiri, S.H. Ahmadi, et al., Dynamic induction of pro-angiogenic milieu after transplantation of marrow-derived mesenchymal stem cells in experimental myocardial infarction, Int. J. Cardiol. 173 (3) (2014) 453–466.

[17] C. Toma, M.F. Pittenger, K.S. Cahill, et al., Human mesenchymal stem cells differentiate to a cardiomyocyte phenotype in the adult murine heart, Circulation 105 (1) (2002) 93–98.

[18] M. Mirotsou, Z. Zhang, A. Deb, et al., Secreted frizzled related protein 2 (Sfrp2) is the key Akt-mesenchymal stem cell-released paracrine factor mediating myocardial survival and repair, Proc. Natl. Acad. Sci. U. S. A. 104 (5) (2007) 1643–1648.

[19] Y. Zhang, D. Wang, K. Cao, et al., Rat induced pluripotent stem cells protect H9C2 cells from cellular senescence via a paracrine mechanism, Cardiology 128 (1) (2014) 43–50.

[20] P. Musialek, L. Tekieli, M. Kostkiewicz, et al., Randomized transcoronary delivery of CD34(+) cells with perfusion versus stop-flow method in patients with recent myocardial infarction: early cardiac retention of (9)(9)(m)Tc-labeled cells activity, J. Nucl. Cardiol. 18 (1) (2011) 104–116.

[21] R. Zamilpa, M.M. Navarro, I. Flores, et al., Stem cell mechanisms during left ventricular remodeling post-myocardial infarction: repair and regeneration, World J. Cardiol. 6 (7) (2014) 610–620.

[22] S. Janssens, C. Dubois, J. Bogaert, et al., Autologous bone marrow-derived stem-cell transfer in patients with ST-segment elevation myocardial infarction: double-blind, randomised controlled trial, Lancet 367 (9505) (2006) 113–121.

[23] D.M. Leistner, U. Fischer-Rasokat, J. Honold, et al., Transplantation of progenitor cells and regeneration enhancement in acute myocardial infarction (TOPCARE-AMI): final 5-year results suggest long-term safety and efficacy, Clin. Res. Cardiol. 100 (10) (2011) 925–934.

[24] J.H. Traverse, T.D. Henry, S.G. Ellis, et al., Effect of intracoronary delivery of autologous bone marrow mononuclear cells 2 to 3 weeks following acute myocardial infarction on left ventricular function: the LateTIME randomized trial, JAMA 306 (19) (2011) 2110–2119.

[25] K.C. Wollert, G.P. Meyer, J. Lotz, et al., Intracoronary autologous bone-marrow cell transfer after myocardial infarction: the BOOST randomised controlled clinical trial, Lancet 364 (9429) (2004) 141–148.

[26] K. Lunde, S. Solheim, S. Aakhus, et al., Intracoronary injection of mononuclear bone marrow cells in acute myocardial infarction, N. Engl. J. Med. 355 (12) (2006) 1199–1209.

[27] A.R. Chugh, G.M. Beache, J.H. Loughran, et al., Administration of cardiac stem cells in patients with ischemic cardiomyopathy: the SCIPIO trial: surgical aspects and interim analysis of myocardial function and viability by magnetic resonance, Circulation 126 (11 Suppl. 1) (2012) S54–S64.

[28] B. Assmus, A. Rolf, S. Erbs, et al., Clinical outcome 2 years after intracoronary administration of bone marrow-derived progenitor cells in acute myocardial infarction, Circ. Heart Fail. 3 (1) (2010) 89–96.

[29] V. Schachinger, S. Erbs, A. Elsasser, et al., Intracoronary bone marrow-derived progenitor cells in acute myocardial infarction, N. Engl. J. Med. 355 (12) (2006) 1210–1221.

[30] A. Schaefer, C. Zwadlo, M. Fuchs, et al., Long-term effects of intracoronary bone marrow cell transfer on diastolic function in patients after acute myocardial infarction: 5-year results from the randomized-controlled BOOST trial—an echocardiographic study, Eur. J. Echocardiogr. 11 (2) (2010) 165–171.

[31] J. Salamon, D. Wicklein, M. Didie, et al., Magnetic resonance imaging of single co-labeled mesenchymal stromal cells after intracardial injection in mice, Rofo 186 (4) (2014) 367–376.

[32] K. Yang, P. Xiang, C. Zhang, et al., Magnetic resonance evaluation of transplanted mesenchymal stem cells after myocardial infarction in swine, Can. J. Cardiol. 27 (6) (2011) 818–825.

[33] E. Elhami, B. Dietz, B. Xiang, et al., Assessment of three techniques for delivering stem cells to the heart using PET and MR imaging, EJNMMI Res. 3 (1) (2013) 72.

[34] J.J. Yang, Z.Q. Liu, J.M. Zhang, et al., Real-time tracking of adipose tissue-derived stem cells with injectable scaffolds in the infarcted heart, Heart Vessels 28 (3) (2013) 385–396.

[35] C. Templin, R. Zweigerdt, K. Schwanke, et al., Transplantation and tracking of human-induced pluripotent stem cells in a pig model of myocardial infarction: assessment of cell survival, engraftment, and distribution by hybrid single photon emission computed tomography/computed tomography of sodium iodide symporter transgene expression, Circulation 126 (4) (2012) 430–439.

[36] J. Terrovitis, K.F. Kwok, R. Lautamaki, et al., Ectopic expression of the sodium-iodide symporter enables imaging of transplanted cardiac stem cells in vivo by single-photon emission computed tomography or positron emission tomography, J. Am. Coll. Cardiol. 52 (20) (2008) 1652–1660.

[37] M. Wildgruber, F.K. Swirski, A. Zernecke, Molecular imaging of inflammation in atherosclerosis, Theranostics 3 (11) (2013) 865–884.

[38] E.A. Osborn, F.A. Jaffer, The advancing clinical impact of molecular imaging in CVD, JACC Cardiovasc. Imaging 6 (12) (2013) 1327–1341.

[39] M.C. Press, F.A. Jaffer, Molecular intravascular imaging approaches for atherosclerosis, Curr. Cardiovasc. Imaging Rep. 7 (10) (2014) 9293.

[40] D.E. Sosnovik, M. Nahrendorf, N. Deliolanis, et al., Fluorescence tomography and magnetic resonance imaging of myocardial macrophage infiltration in infarcted myocardium in vivo, Circulation 115 (11) (2007) 1384–1391.

[41] F.K. Swirski, M. Nahrendorf, M. Etzrodt, et al., Identification of splenic reservoir monocytes and their deployment to inflammatory sites, Science 325 (5940) (2009) 612–616.

[42] C. Vinegoni, P. Fumene Feruglio, D. Razansky, et al., Mapping molecular agents distributions in whole mice hearts using born-normalized optical projection tomography, PLoS One 7 (4) (2012) e34427.

[43] P. Mohajerani, S. Tzoumas, A. Rosenthal, et al., Optical and optoacoustic model-based tomography: theory and current challenges for deep tissue imaging of optical contrast, IEEE Signal Process Mag. 32 (1) (2015) 88–100.

[44] V. Ntziachristos, Going deeper than microscopy: the optical imaging frontier in biology, Nat. Methods 7 (8) (2010) 603–614.

[45] A. Ale, V. Ermolayev, E. Herzog, et al., FMT-XCT: in vivo animal studies with hybrid fluorescence molecular tomography-X-ray computed tomography, Nat. Methods 9 (6) (2012) 615–620.

[46] P. Mohajerani, A. Hipp, Marian Willner, et al., FMT-PCCT: Hybrid fluorescence molecular tomography—X-ray phase-contrast CT imaging of mouse models, IEEE Trans. Med. Imaging 33 (7) (2014).

[47] V. Ntziachristos, D. Razansky, Molecular imaging by means of multispectral optoacoustic tomography (MSOT), Chem. Rev. 110 (5) (2010) 2783–2794.

[48] D. Razansky, A. Buehler, V. Ntziachristos, Volumetric real-time multispectral optoacoustic tomography of biomarkers, Nat. Protoc. 6 (8) (2011) 1121–1129.

[49] A. Taruttis, M. Wildgruber, K. Kosanke, et al., Multispectral optoacoustic tomography of myocardial infarction, Photoacoustics 1 (1) (2013) 3–8.

[50] A. Taruttis, E. Herzog, D. Razansky, et al., Real-time imaging of cardiovascular dynamics and circulating gold nanorods with multispectral optoacoustic tomography, Opt. Express 18 (19) (2010) 19592–19602.

[51] F.M. Youniss, G. Sundaresan, L.J. Graham, et al., Near-infrared imaging of adoptive immune cell therapy in breast cancer model using cell membrane labeling, PLoS One 9 (10) (2014) e109162.

[52] X. Du, X. Wang, N. Ning, et al., Dynamic tracing of immune cells in an orthotopic gastric carcinoma mouse model using near-infrared fluorescence live imaging, Exp. Ther. Med. 4 (2) (2012) 221–225.

[53] N.I.O. Health, Guide for the Care and Use of Laboratory Animals, National Academies, 1985.

[54] M.T. Berninger, G. Wexel, E.J. Rummeny, et al., Treatment of osteochondral defects in the rabbit's knee joint by implantation of allogeneic mesenchymal stem cells in fibrin clots, J. Vis. Exp. 75 (2013).

[55] R. Haugland, Carlsbad, Laboratory Manual from Molecular Probes, Invitrogen Corporation, Carlsbad, CA, 2003 Section 14.4.

[56] J.M. Lee, J.K. Yoo, H. Yoo, et al., The novel miR-7515 decreases the proliferation and migration of human lung cancer cells by targeting c-Met, Mol. Cancer Res. 11 (1) (2013) 43–53.

[57] A. Nedopil, C. Klenk, C. Kim, et al., MR signal characteristics of viable and apoptotic human mesenchymal stem cells in matrix-associated stem cell implants for treatment of osteoarthritis, Invest. Radiol. 45 (10) (2010) 634–640.

[58] R.B. Schulz, A. Ale, A. Sarantopoulos, et al., Hybrid system for simultaneous fluorescence and X-ray computed tomography, IEEE Trans. Med. Imaging 29 (2) (2010) 465–473.

[59] A. Sarantopoulos, G. Themelis, V. Ntziachristos, Imaging the bio-distribution of fluorescent probes using multispectral epi-Illumination cryoslicing imaging, Mol. Imaging Biol. 13 (5) (2011) 874–885.

[60] A. Buehler, E. Herzog, D. Razansky, et al., Video rate optoacoustic tomography of mouse kidney perfusion, Opt. Lett. 35 (14) (2010) 2475–2477.

[61] M. Nahrendorf, D.E. Sosnovik, P. Waterman, et al., Dual channel optical tomographic imaging of leukocyte recruitment and protease activity in the healing myocardial infarct, Circ. Res. 100 (8) (2007) 1218–1225.

[62] A. Ale, F. Siebenhaar, K. Kosanke, et al., Cardioprotective C-kit(+) bone marrow cells attenuate apoptosis after acute myocardial infarction in mice—in-vivo assessment with fluorescence molecular imaging, Theranostics 3 (11) (2013) 903–913.

[63] C.J. Goergen, D.E. Sosnovik, From molecules to myofibers: multiscale imaging of the myocardium, J. Cardiovasc. Transl. Res. 4 (4) (2011) 493–503.

[64] A. Oraevsky, A. Karabutov, Optoacoustic tomography, in: T. Vo-Dinh (Ed.), Biomedical Photonics Handbook, CRC Press LLC, 2003, pp. 1–34.

[65] M. Xu, L.V. Wang, Photoacoustic imaging in biomedicine, Rev. Sci. Instrum. 77 (4) (2006) 041101.

[66] J.V. Jokerst, M. Thangaraj, P.J. Kempen, et al., Photoacoustic imaging of mesenchymal stem cells in living mice via silica-coated gold nanorods, ACS Nano 6 (7) (2012) 5920–5930.
[67] D. Razansky, C. Vinegoni, V. Ntziachristos, Multispectral photoacoustic imaging of fluorochromes in small animals, Opt. Lett. 32 (19) (2007) 2891–2893.
[68] M.D.D. Razansky, C. Vinegoni, R. Ma, N. Perrimon, R.W. Köster, V. Ntziachristos, Multispectral opto-acoustic tomography of deep-seated fluorescent proteins in vivo, Nat. Photonics 3 (7) (2009) 412–417.
[69] M. Eghtedari, A. Oraevsky, J.A. Copland, et al., High sensitivity of in vivo detection of gold nanorods using a laser optoacoustic imaging system, Nano Lett. 7 (7) (2007) 1914–1918.
[70] M. Eisenblatter, J. Ehrchen, G. Varga, et al., In vivo optical imaging of cellular inflammatory response in granuloma formation using fluorescence-labeled macrophages, J. Nucl. Med. 50 (10) (2009) 1676–1682.
[71] R.R. Makkar, R.R. Smith, K. Cheng, et al., Intracoronary cardiosphere-derived cells for heart regeneration after myocardial infarction (CADUCEUS): a prospective, randomised phase 1 trial, Lancet 379 (9819) (2012) 895–904.
[72] J. Roncalli, F. Mouquet, C. Piot, et al., Intracoronary autologous mononucleated bone marrow cell infusion for acute myocardial infarction: results of the randomized multicenter BONAMI trial, Eur. Heart J. 32 (14) (2011) 1748–1757.
[73] N. Azene, Y. Fu, J. Maurer, et al., Tracking of stem cells in vivo for cardiovascular applications, J. Cardiovasc. Magn. Reson. 16 (2014) 7.
[74] L.J. Mortensen, O. Levy, J.P. Phillips, et al., Quantification of Mesenchymal Stem Cell (MSC) delivery to a target site using in vivo confocal microscopy, PLoS One 8 (10) (2013) e78145.
[75] H. Cho, G.L. Indig, J. Weichert, et al., In vivo cancer imaging by poly(ethylene glycol)-b-poly(varepsilon-caprolactone) micelles containing a near-infrared probe, Nanomedicine 8 (2) (2012) 228–236.
[76] C. Baligand, K. Vauchez, M. Fiszman, et al., Discrepancies between the fate of myoblast xenograft in mouse leg muscle and NMR label persistency after loading with Gd-DTPA or SPIOs, Gene Ther. 16 (6) (2009) 734–745.
[77] J. Terrovitis, M. Stuber, A. Youssef, et al., Magnetic resonance imaging overestimates ferumoxide-labeled stem cell survival after transplantation in the heart, Circulation 117 (12) (2008) 1555–1562.
[78] Y. Amsalem, Y. Mardor, M.S. Feinberg, et al., Iron-oxide labeling and outcome of transplanted mesenchymal stem cells in the infarcted myocardium, Circulation 116 (Suppl. 11) (2007) I38–45.
[79] E. Pawelczyk, E.K. Jordan, A. Balakumaran, et al., In vivo transfer of intracellular labels from locally implanted bone marrow stromal cells to resident tissue macrophages, PLoS One 4 (8) (2009) e6712.
[80] T.D. Henning, M.F. Wendland, D. Golovko, et al., Relaxation effects of ferucarbotran-labeled mesenchymal stem cells at 1.5T and 3T: discrimination of viable from lysed cells, Magn. Reson. Med. 62 (2) (2009) 325–332.
[81] L.M. Ricles, S.Y. Nam, E.A. Trevino, et al., A dual gold nanoparticle system for mesenchymal stem cell tracking, J. Mater. Chem. B: Mater. Biol. Med. 2 (46) (2014) 8220–8230.
[82] J. Jin, S.I. Jeong, Y.M. Shin, et al., Transplantation of mesenchymal stem cells within a poly(lactide-*co*-epsilon-caprolactone) scaffold improves cardiac function in a rat myocardial infarction model, Eur. J. Heart Fail. 11 (2) (2009) 147–153.
[83] S.Y. Nam, L.M. Ricles, L.J. Suggs, et al., In vivo ultrasound and photoacoustic monitoring of mesenchymal stem cells labeled with gold nanotracers, PLoS One 7 (5) (2012) e37267.
[84] L. Wang, X. Hu, W. Zhu, et al., Increased leptin by hypoxic-preconditioning promotes autophagy of mesenchymal stem cells and protects them from apoptosis, Sci. China Life Sci. 57 (2) (2014) 171–180.
[85] U. Saini, R.J. Gumina, B. Wolfe, et al., Preconditioning mesenchymal stem cells with caspase inhibition and hyperoxia prior to hypoxia exposure increases cell proliferation, J. Cell. Biochem. 114 (11) (2013) 2612–2623.
[86] W.E. Wang, D. Yang, L. Li, et al., Prolyl hydroxylase domain protein 2 silencing enhances the survival and paracrine function of transplanted adipose-derived stem cells in infarcted myocardium, Circ. Res. 113 (3) (2013) 288–300.
[87] D. Luger, M.J. Lipinski, P.C. Westman, et al., Intravenously-delivered mesenchymal stem cells: systemic anti-inflammatory effects improve left ventricular dysfunction in acute myocardial infarction and ischemic cardiomyopathy, Circ. Res. (2017), doi:http://dx.doi.org/10.1161/CIRCRESAHA.117.310599 Feb 23 [Epub ahead of print] PMID: 28232595.
[88] I.M. Barbash, P. Chouraqui, J. Baron, et al., Systemic delivery of bone marrow-derived mesenchymal stem cells to the infarcted myocardium: feasibility, cell migration, and body distribution, Circulation 108 (7) (2003) 863–868.

Markus T. Berninger studied medicine at the Technical University in Munich. He started his orthopedic residency at the Department of Orthopedic Sports Medicine, Klinikum rechts der Isar, Technical University Munich where he also received his doctorate in 2013. Since 2014 he works as a resident at the Department of Trauma and Orthopedic Surgery, Trauma Center Murnau, Germany. His research focuses on tissue engineering and translation of novel (stem cell) imaging technologies especially in the setting of musculoskeletal questions and cartilage repair.

Pouyan Mohajerani studied electrical engineering at Sharif University of Technology and later received his M. Sc. in electrical engineering from Georgia Institute of Technology in 2004. He is currently a Ph.D. student in the Institute for Biological and Medical Imaging (IBMI) at Technical University Munich and Helmholtz Zentrum Muenchen, Munich, Germany.H is current research interests are in the general fields of signal and image processing.

Moritz Wildgruber studied medicine at the universities of Munich (TU), New York and Bern and graduated in 2007. Subsequently he went for a postdoctoral research fellowship from 2007 to 2008 at the Massachusetts General Hospital where he joined the lab of Ralph Weissleder to work on Imaging of the innate and adaptive immune system in cardiovascular disease. After his residency and fellowship training in Radiology in Munich and Regensburg he became full professor of radiology at the University Hospital of Münster, where he is a senior attending in interventional radiology and in parallel heads a research group in Translational Radiology.

Nicolas Beziere studied chemistry and pharmacology at the University of Pharmacy in Lille, France, where he received his doctorate degree. After a first post-doctoral research on reactive oxygen species spectroscopy and imaging at the University Descartes in Paris, France, he joined the Institute for Biological and Medical Imaging in Munich, Germany, to investigate the preclinical potential of photoacoustic imaging as the group leader of the Optoacoustic Theranostics team. His main activities are centered on the development of nanomedicine based diagnosis, therapy and therapy monitoring through the development of advanced imaging tools.

Melanie A. Kimm studied biology at the Ludwigs-Maximillians-Universität (LMU) in Munich, Germany and the Netherlands Cancer Institute, Amsterdam, Holland before she received her doctorate in medical biology from the LMU, Munich, Germany. Currently, she is an Associate project leader and Senior Scientist at the Department of Radiology at the Klinikum rechts der Isar, Technical University Munich, Germany. Her research activities include cell labeling for in vivo tracking as well as setting up preclinical models for molecular imaging of inflammation and immunotherapies using CT, MRI and optoacoustic imaging.

Xiaopeng Ma is currently a PhD student in the Institute for Biological and Medical Imaging (IBMI) at Technical University Munich and Helmholtz Zentrum Munich, Germany. He received his BS degree in electronic science and technology in 2008 and later received his MSc degree in electrical engineering in 2011, both from Xidian University, China. His current research interests are fluorescence molecular tomography, x-ray computed tomography and in-vivo biomedical imaging applications.

Bernhard Haller studied statistics at the Ludwig-Maximilians-Universität (LMU) in Munich, Germany. He has since worked as research assistant and statistical consultant at the Institute of Medical Statistics and Epidemiology of the Technical University of Munich (TUM) and received his doctorate degree in statistics from the LMU. His current research is focused on the development and evaluation of statistical methods for the analysis of survival data in the presence of competing risks and on methods for identification and estimation of biomarker-treatment interactions from data collected in randomized controlled trials.

Megan J. Fleming studied medicine at the Technical University of Munich, Germany, the University of Lausanne, Switzerland and Newcastle University, Great Britain. She is now pursuing her medical doctorate degree at the Department of Orthopedic Sports Medicine. The Focus of which is in vivo stem cell tracking, currently examining SPIO labelled stem cells for MRI tracking and the impact of said labelling on stem cell differentiation potential.

Stephan Vogt has a medical degree from the University of Essen, Germany. He did his PhD thesis at the institute of pharmacology (University of Essen). He started his orthopedic career at the University of Heidelberg, Germany. For three years he worked as a postdoc at the institute of molecular pharmacology in Heidelberg, Germany. After this time he continued his orthopedic career at the TU Munich, Germany. He received his habilitation for orthopedic and trauma surgery in 2009 and became a professor in 2015. Since 2012 he is head of the sports orthopedic department in Augsburg (Hessing Stiftung) and since 2015 head of the Hessing Stiftung. His scientific topics are basic cartilage research, gene transduction, growth factors, cell signaling and clinical studies regarding regenerative medicine.

Martina Anton studied biology at the University of Konstanz, Germany, where she received her diploma and doctoral degree in microbiology. She completed her postdoc at the Departments of Biology and Pathology at McMaster University Hamilton, Canada in the field of adenoviral vector technology. She is currently senior researcher and leads the group of viral gene transfer at the Institute of Experimental Oncology and Therapy Research, Klinikum rechts der Isar, Technical University Munich. Her research focuses on optimizing gene transfer by adeno- and lentiviral vectors in basic research, oncological and regenerative settings. She has experience in genetic, nanoparticle and combined labeling of primary cells for imaging and therapeutic approaches.

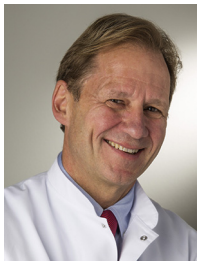

Andreas B. Imhoff graduated in medicine from Basel University in 1980 and did his residency in General Surgery, Traumatology and Knee surgery in Davos and Basel, Switzerland. He completed his orthopedic residency at the Balgrist University Hospital, Zurich, where he was head of different departments for knee, shoulder and sports medicine after 1987. From 1994 to 1995 he did a clinical and research fellowship at the Center of Sports Medicine and the Musculoskeletal Research Center, University of Pittsburgh, PA, USA. Since 1996 he is director and chairman of the Department of Orthopedic Sports Medicine, Klinikum Rechts der Isar, Technical University Munich. His research focuses on clinical and experimental studies regarding tissue engineering and regenerative medicine as well as biomechanical and clinical trials of musculoskeletal injuries.

Vasilis Ntziachristos studied electrical engineering at Aristotle University in Thessaloniki, Greece and received his Master's and Doctorate degrees from the Bioengineering Department of the University of Pennsylvania, USA. After completing a postdoc at the Center for Molecular Imaging Research (CMIR) at Harvard Medical School, he served as an instructor and then assistant professor and director of the Laboratory for Bio-Optics and Molecular Imaging at Harvard University and Massachusetts General Hospital, Boston, USA. He is currently a Professor of Medicine, Professor of Electrical Engineering and Chair for Biological Imaging (CBI) at the Technical University Munich and the Director of the Institute for Biological and Medical Imaging (IBMI) at the Helmholtz Zentrum Munich, Germany. His research concentrates on basic research and translation of novel optical and optoacoustic in vivo imaging for addressing unmet biological and clinical needs.

Reinhard Meier studied medicine in Munich, Nice and San Francisco and received his doctorate from the Technical University Munich. After completing a postdoc program in Molecular Imaging at the University of California San Francisco, he served as a resident in Diagnostic and Interventional Radiology at Klinikum rechts der Isar, Technical University Munich. He is currently a Professor of Radiology and director of the Translational Molecular Imaging Lab at the Department of Radiology, Klinikum rechts der Isar, Technical University Munich. His laboratory concentrates on basic research and translation of new imaging technologies especially in the area of oncology and inflammation.

Tobias D. Henning studied medicine at the universities of Freiburg, Hamburg, Grenoble and received his doctorate from the Albert Ludwigs-University in Freiburg, Germany. He completed his residency in Diagnostic Radiology and in Diagnostic and Interventional Neuroradiology at the Technical University of Munich and the University of Cologne as well as a postdoctoral fellowship in Molecular Imaging at the University of California, San Francisco. Tobias Henning works as a radiologist for Interventional and Diagnostic Neuroradiology in Trier, Germany. His research focuses on stem cell imaging techniques in the setting of tissue engineering.